High-Aspect-Ratio Metal Microfabrication by Nickel Electroplating of Patterned Carbon Nanotube Forests

Lawrence K. Barrett, Dallin J. Barton, Steven G. Noyce, David D. Allred, Richard R. Vanfleet, and Robert C. Davis

***Abstract*— High-aspect-ratio metallic microstructures have a variety of potential applications in sensing and actuation. However, fabrication remains a challenge. We have fabricated nickel microstructures with over 20:1 aspect ratios by electroplating patterned carbon-coated carbon-nanotube forests using a nickel chloride bath. Pulse plating allows nickel ions to diffuse into the interior of the forest during off portions of the cycle. Done properly, this solves the problem of the formation of an external crust, which otherwise blocks nickel deposition in the interior of the structures. Thus, densities of 86 ± 3% of bulk Ni for the composite structures are achieved. Cantilever structures do not yield under load, but break. Measurements of the material properties of this composite material indicate an elastic modulus of ∼42 GPa and a strength of 400 MPa. We demonstrate the utility of this method with an external field magnetic actuator consisting of a proof mass and two flexures. We achieved 1-mN actuation forces. [2014-0274]**

***Index Terms*— Magnetic, carbon, microelectromechanical, nickel, aspect ratio.**

I. Introduction

MEMS SENSORS and actuators are used in smart phones, automobiles, gaming systems, military equipment and a wealth of other applications. In these devices, high-aspect-ratios (HAR) are often desirable. HAR increase mechanical robustness and surface area for capacitive actuation and sensing, while decreasing the out-of-plane motion and, consequently, the crosstalk of these devices [1]. Methods for fabricating high-aspect-ratio devices include: subtractive processes such as deep reactive ion etching (DRIE) [2], additive processes, such as LIGA [3], UV-LIGA [4], and carbon nanotube templated microfabrication (CNT-M) [5]. Even though each of these processes have been somewhat successful in fabricating high-aspect-ratio microstructures, creating similar structures from metals remains a challenge (with the exception of titanium, which has found success using DRIE [6]).

Metal MEMS advantages include: high density, high yield strength, high yield strain, as well as high thermal and electrical conductivity. Each of these properties enables higher performance for MEMS devices. Additionally, ferromagnetic metals can enable actuation devices that are not currently possible. Presently, most actuation is done capacitively or by piezoelectric materials [7]. Magnetic actuation can achieve larger forces at larger distances. Magnetic actuation forces begin to be stronger than capacitive forces at distances above about 2 μm [8], and magnetism can be used to actuate devices at millimeter or even centimeter distances.

Because magnetic actuators can be actuated at large distances, the drive magnet (or electromagnet) can be located off chip. These devices are referred to as external field magnetic actuators. They have two main advantages: 1) The drive magnetic can simultaneously actuate multiple devices, and 2) the actuator can be physically isolated. Examples include microfluidic mixers [9], microfluidic pumps [10], mirror arrays [11], [12], biological implants, and microrobotics for noninvasive surgery [13].

Currently, most external field magnetic actuators are made by depositing a magnetic layer onto a frame made from a non-magnetic material. This is due to the difficulty of making precise structures directly from magnetic material. These layers are generally not thicker than 5 μm because of deformation and poor adhesion caused by intrinsic stresses. This limits the force of actuation because the force scales linearly with the volume of the ferromagnetic material [14]. HAR ferromagnetic devices are a promising alternative because they can have large volumes without sacrificing precise features or small footprints.

LIGA and UV-LIGA have been the most successful methods for fabricating metal MEMS [3]. LIGA uses synchrotron radiation to expose a high-aspect-ratio photoresist. After the resist is developed, the holes are filled via electroforming, a special version of electroplating designed to deposit thicker layers. A major drawback of this process is the synchrotron expense [3].

UV-LIGA is a variation of LIGA, It uses photoresists such as SU-8 and KMPR which can be developed by ultraviolet light. Consequently, UV-LIGA avoids the expense of using

Manuscript received September 4, 2014; revised November 22, 2014; accepted December 4, 2014. This work was supported in part by the Department of Physics and Astronomy, Brigham Young University, Provo, UT, USA, and in part by the Brigham Young University Office of Research and Creative Activities. Subject Editor R. Maboudian.

The authors are with the Department of Physics and Astronomy, Brigham Young University, Provo, UT 84602 USA (e-mail: barrett.lawrence@gmail.com; dallin.barton@gmail.com; steven.noyce@gmail.com; allred@byu.edu; rrv3@physics.byu.edu; davis@byu.edu).

Color versions of one or more of the figures in this paper are available online at http://ieeexplore.ieee.org.

Digital Object Identifier 10.1109/JMEMS.2015.2395954

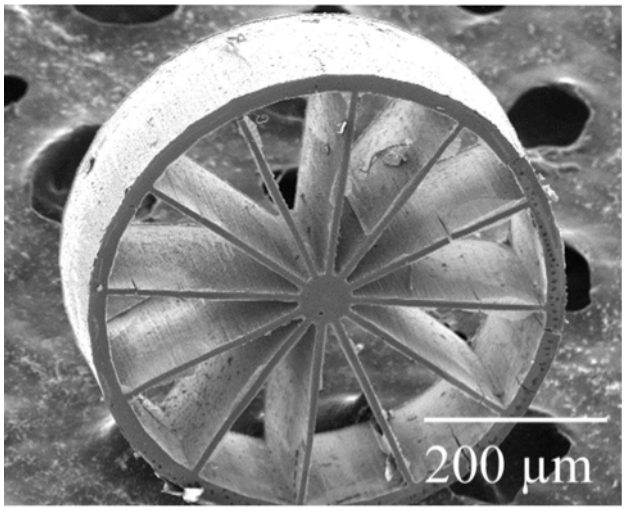

Fig. 1. An SEM micrograph of a wagon wheel structure made by electroplating carbon-coated CNTs. The spokes are 10 μm wide and the wheel is over 200 μm wide.

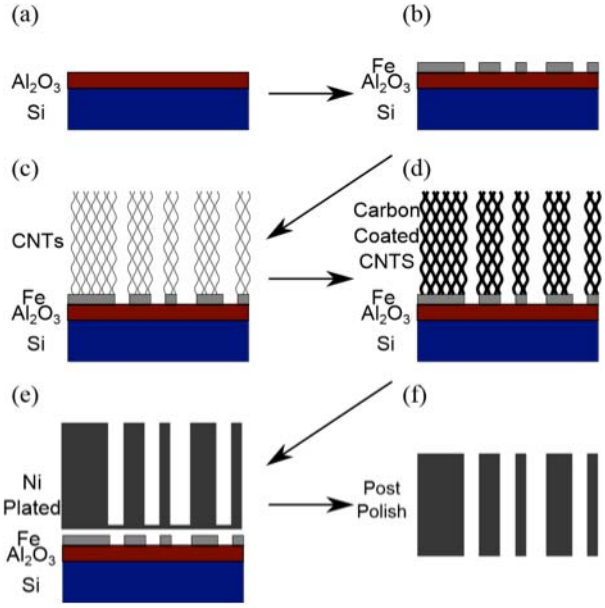

Fig. 2. Process diagram for nickel CNT-M. (a) A 30 nm layer of Al_2O_3 is e-beam evaporated on a silicon wafer. (b) Liftoff is used to produce a patterned 7 nm Fe layer. The Fe serves as catalyst for CNT growth. (c) Vertically aligned CNTs grow from the Fe catalyst. (d) They are coated with a thin (approx. 20 nm) layer of nanocrystalline carbon by atmospheric pressure CVD at 900 °C. (e) The forest is electroplated with Ni until it is filled. The electroplating usually causes the structure to detach from the wafer. If it did not detach, it was released by etching in 30% KOH. (f) A thin floor layer forms on the wafer during plating. The layer is removed by mechanical polishing with a 3 μm lapping film.

a synchrotron. Photoresist structures with high-aspect-ratios have been obtained [15]–[17]; however, the metal structures that are made by filling these photoresist molds by electroforming have significantly lower aspect-ratios because of electroforming challenges. These challenges include voids in the deposit [17], nonuniform thickness of deposits [18], long deposition times, and deformation or cracking due to internal stress in the deposit [19], [20]. Deformation from stress is a major obstacle to making HAR metallic devices with freestanding parts [21]. Both, UV-LIGA and LIGA have other drawbacks including: deformation due to stress in the photoresist [22] and the difficulty of removing the photoresist [23].

Here, we show CNT-M can be extended to metals, and that it addresses challenges of LIGA and UV-LIGA. Particularly, it exhibits very little deformation due to stress on movable HAR parts. In CNT-M, vertically aligned CNT forests are grown from a patterned iron catalyst. The process is like extruding a 3D structure from a 2D pattern. The CNT forest grows into a MEMS geometry but has no structural integrity. As a result, it is infiltrated and filled with another material by CVD (chemical vapor deposition) [5]. Others have successfully infiltrated forests with carbon, silicon nitride and amorphous silicon [5], [24], but attempts to infiltrate with metals by CVD have met limited success [25], [26].

We successfully infiltrated with metals by means of an electroplating process. The patterning in this process is significantly less expensive than LIGA because it can be done with standard photolithography. It also can be done at aspect ratios greater than 20:1 (fig. 1) without significant voids. The secret to void-free infiltration is pulse deposition. The sticking coefficient is the probability that an adatom, an atom that is being deposited, deposits instead of rebounding off the forest. Using pulsed electroplating we can create a low effective sticking coefficient because ions will only deposit when there is sufficient potential applied to the forest to drive the chemical reduction of the nickel containing ion, depositing the metal.

II. Methods

A. Sample Fabrication

As seen in fig. 2, the process outlined by Hutchinson et al. was followed to prepare the samples for electroplating [5]. Silicon wafers were coated in 30 nm of Al_2O_3. Photoresist was then patterned on the wafer via contact photolithography. A 7 nm layer of iron (Fe) was thermally evaporated on the wafer, and the photoresist was subsequently stripped by sonication in NMP, leaving behind a patterned layer of Fe which served as the catalyst for CNT growth [25]. The next two steps were performed in the same deposition tube. First, vertically aligned CNTs were grown by CVD. The sample was placed in a 7/8 in. ID tube furnace, heated to 750 °C. Then, 220 sccm of H_2 was flowed while the furnace was heated to reduce the catalyst. After the furnace reached 750 °C, H_2 flow was continued at the same rate and 260 sccm of C_2H_4 was added. Since the resulting CNT structures are weak and can deform in the electroplating bath, a thin nanocrystalline carbon layer was deposited. This was done immediately after CNT growth by increasing the temperature to 900 °C for two minutes while continuing the same gas flow rates.

B. Electroplating

After the forests were grown and strengthened, they were filled with nickel by pulse electroplating. The electroplating

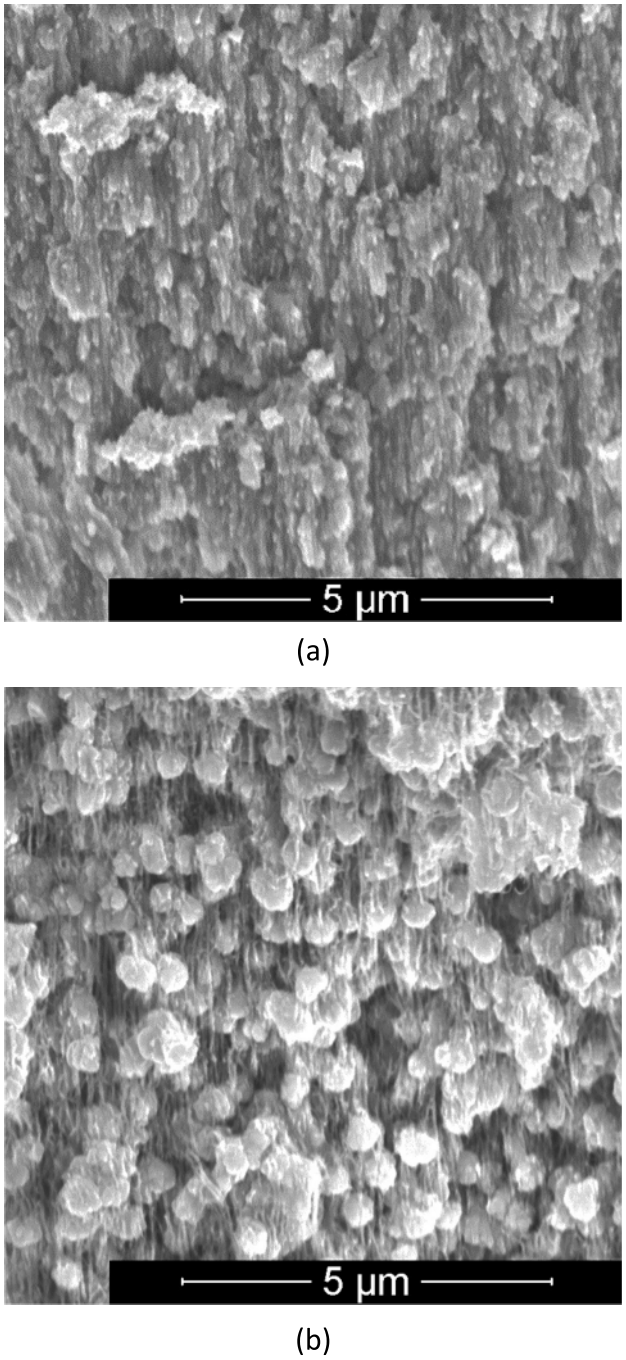

Fig. 3. SEM micrographs of the cross section of the interior (broken open) of an electroplated CNT structure with an array of 10 μm pores to facilitated diffusion (a) near the top of the sample (b) near the bottom of the sample and the substrate. The structure is over 200 μm tall. It was plated in a $NiCl_2$ bath at 8 A/cm^3 and a 3 ms on time, but the off time was only 6 ms. It can be seen that there is significantly more nickel deposited near the top, but little near the bottom. This is most evident from the CNTs being visible near the bottom, but not near the top.

must be tuned to avoid there being more deposition on the wafer than at the substrate, as seen in fig. 3. It is suspected that this nonuniform deposition occurs because the electroplating depletes the metal ions from the solution faster than they can be replenished by diffusion. To increase diffusion, both the composition of the bath and the rest time in between plating pulses were changed. An aqueous $NiCl_2$ solution was found to enable sufficiently rapid diffusion. The solution was composed of 125 g/l $NiCl_2$ $6H_2O$ (as nickel(II) chloride hexahydrate) and 12.5 g/l boric acid.

Current per area is the traditional measure of current density, but it is a difficult metric to use with CNT forests. Measuring the surface area of a CNT forest is not trivial. Furthermore, this measurement does not remain constant throughout the plating process. As metal is deposited on the CNTs the surface area will rise initially and then fall as the deposits grow together. The better metric in this case is current per unit volume. All of the samples were plated with 8 A/cm^3 during the on cycle. Prior to electroplating, the samples were treated with ozone.

Because carbon coated CNTs are hydrophobic, air can become trapped in the forest during insertion into the plating bath. This trapped air results in voids. Ozone treatment has been shown to change CNTs from hydrophobic to hydrophilic [27]. The samples were ozonated following the procedure outlined in Jensen et. al for at least 30 min [28]. Electrical contact was made to the sample by touching the top of the carbon coated CNTs with a needle point. After being placed in the solution, the forest was left to sit for 30 min before plating began. During plating, the on cycle was 3 ms and the off cycle was 27 ms, unless otherwise noted. Plating continued for 8.5 hours. The solution was maintained at 50 °C and stirred with a magnetic stir rod. The nickel source was sulfur depolarized nickel discs kept in a titanium basket.

C. Floor Layer

As discussed in Moulton et. al [24], during CNT growth thin beams grow straighter and with more consistent dimensions when there is a nearby CNT guide structure which is also growing [24]. Guide structures were placed 20 μm from the thin beams on the device grown here. While they were not attached to the sample before plating, they became attached during the plating process. During the CVD carbon coating step, a thin layer of conductive carbon was deposited onto the wafer. Nickel deposits both onto this layer and the CNTs, attaching the guide structures to the beams. To remove this thin attachment layer, the sample was polished with a 3 μm lapping film. During the polishing the sample was attached to a piece of glass with cyanoacrylate glue to prevent the beams from breaking. After the floor layer was polished away the sample was allowed to soak in acetone until the glue dissolved, releasing it from the glass.

This step is not ideal for manufacturing, but there is potentially an alternative. If the samples are grown on a thicker insulating layer and the conductive carbon layer is removed, possibly by O_2 plasma etching, the nickel will not deposit on the substrate because there will be no electrical contact to the substrate. This would render the polishing step unnecessary.

III. Material Properties

The structures fill uniformly from top to bottom as seen in figure 4a-b. The structure is largely comprised of nickel a evidenced by the density of the material and the edx spectrum (fig. 4c); however, the resulting composite material

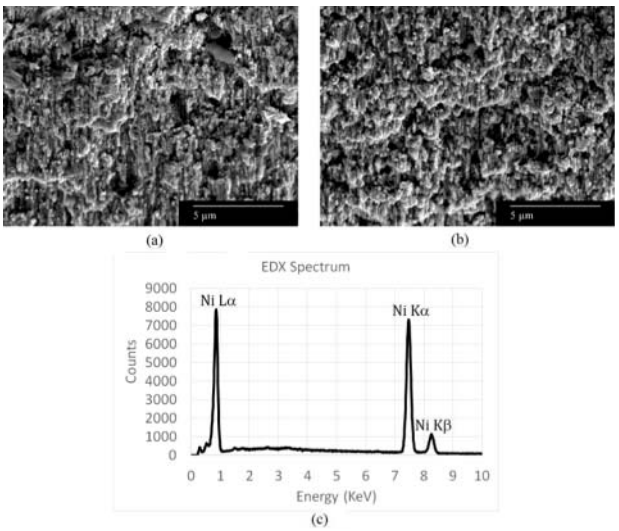

Fig. 4. Analysis of a nickel structure made with CNT-M. SEM micrographs of (a) near the top and (b) near the bottom of the cross section of a nickel structure that has been broken open. The distance between images a and b is greater than 100 μm. It can be qualitatively observed that the nickel deposits uniformly because a and b show the same level of deposition. (c) Edx spectrum taken on top of the sample (not the cross section) at a beam energy of 20 KeV. The edx data implies that the structure is largely nickel because those are the only large peaks.

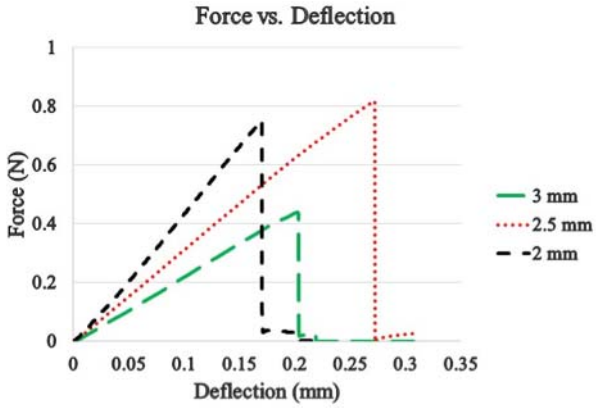

Fig. 5. Force vs. deflection curves for three cantilevers of different lengths. The cantilevers were 190 μm tall and 525 μm wide. It should be noted the material does not yield prior to breaking.

also contains carbon-coated CNTs and some voids. To better understand this composite material for potential uses in MEMS, measurements were made to determine three material properties: density (ρ), elastic modulus (E), and tensile strength (σ).

Several fixed free cantilever beams were fabricated. The force vs. deflection curve was measured using an Instron tabletop tensile testing machine in a manner similar to the methods described in Hanna et. al [29]. Fig. 5 shows the force-deflection curves for 3 cantilevers of different lengths. It should be noted the material does not yield prior to breaking. Consequently, references to tensile strength refer to ultimate and not yield, strength. The elastic modulus and strength was calculated from these curves. The slope of the curve (k) relates to the elastic modulus as shown [7]:

$$E = \frac{4L^3k}{WH^3} \tag{1}$$

where E is the elastic modulus and L, W, and H are the length, width, and height respectively of the cantilever beam. Measurements of the elastic modulus ranged from 20-65 GPa with an average value of 42.4 GPa. Microfabricated nickel from other processes generally has a modulus of about 200 GPa, meaning our structures are significantly more compliant [30], [31]. The tensile strength can be obtained from the force on the beam at breaking and the beam's dimensions [7]:

$$\sigma = \frac{6FL}{WH^2} \tag{2}$$

where F is the force when the beam broke. The strength values ranged from 229-643 MPa. The average value was 383 MPa. The yield strength of annealed bulk nickel is 140-350 MPa [32]. Hence, the material maintains its strength despite being more compliant. It should be noted eq. 2 does not take into account stress concentration which could be quite high because the radius of curvature between the cantilever and the base was less than 10 μm. As a result, the material's tensile strength may be significantly higher. The density was obtained by combining mass and volume measurements. The measured values ranged from 7.3-7.98 g/cm^3. The average value was 7.65 g/cm^3. This is 86% of the density of bulk nickel (8.9 g/cm^3).

IV. External Field Magneticactuator

To demonstrate the utility of this method, an several external field magnetic actuator was constructed. The actuators consisted of a proof mass suspended from a ridged frame by two thin cantilever beams. One of these devices is shown in fig. 6. It has beams that are 1 mm long, 80 μm tall and 12 μm wide. Even though these beams are movable, have a high aspect ratio, and are very long, there is no significant deformation due to stress. One of the devices was cut open with a focused ion beam to show the interior (fig. 6). The cross section does not show any major voids confirming the high densities measured.

To demonstrate actuation, a neodymium magnet was brought within 2-3 mm of the actuator with a field strength of 300 mT as measured by a hall probe at the location of the proof mass. The deflection was observed and measured under an optical microscope as seen in fig. 6.

The device can be modeled as two fixed-guided cantilever beams, and the spring constant can be estimated using the dimensions of the beams and the measured elastic modulus. The spring constant relates to these parameters as follows:

$$k = \frac{2W^3HE}{L^3} \tag{3}$$

where W is the width (12 μm), H is the height (80 μm), and L is the length (1 mm) [7]. The spring constant is about 12 N/m, which yields a force of approximately 1 mN at a displacement of 80 μm. The device has not been optimized

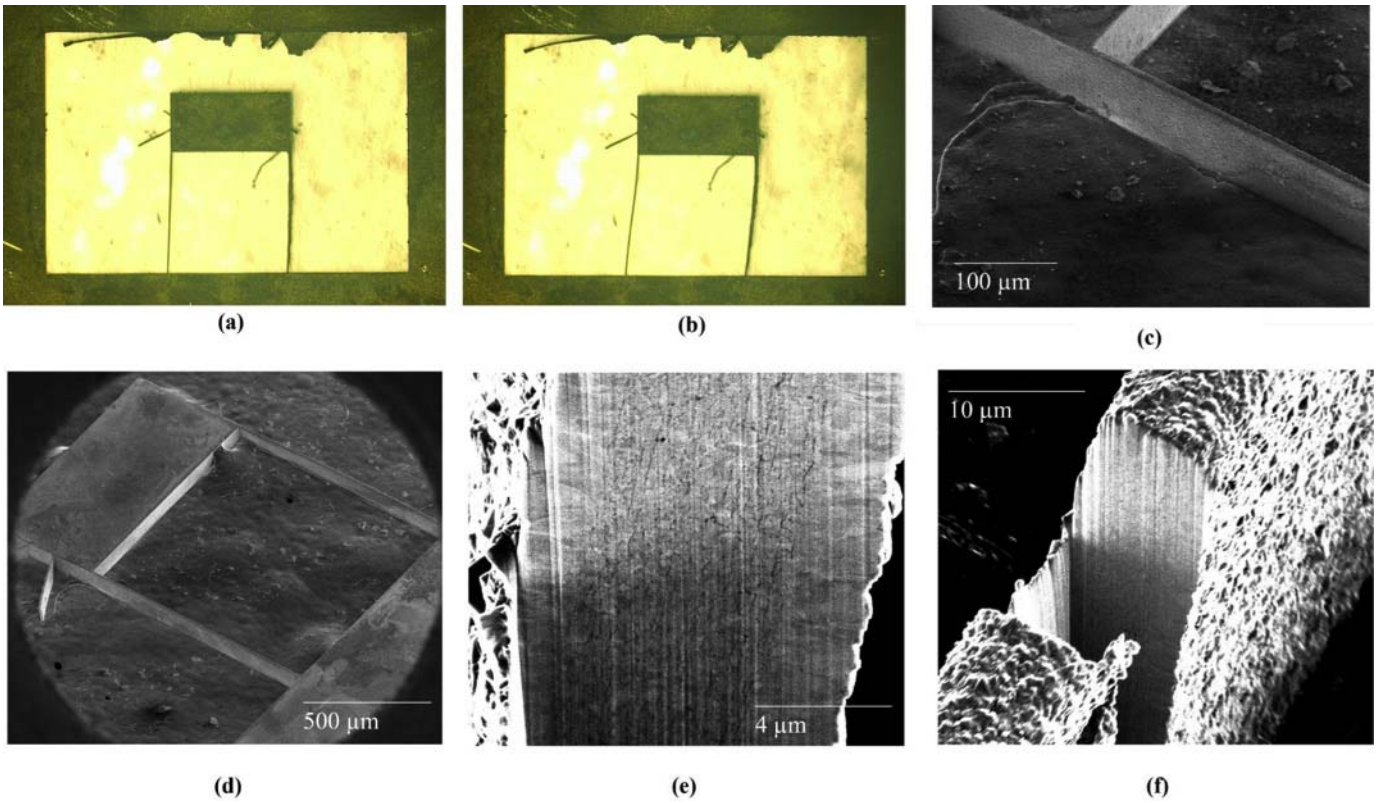

Fig. 6. Images of an external field magnetic actuator: Optical microscope images of the device (a) undeflected and (b) deflecting towards a neodymium magnet. The deflection was approximately 80 μm with the magnet 2-3 mm away. (c) SEM micrograph of part the device seen in figures a and b. The beams are approximately 80 μm tall, 12 μm, and 1 mm long. The structure seen here is attached to carbon tape for imaging. The extra pieces coming off of the proof mass are connectors that were included to help with plating. They were removed mechanically with tweezers. (d) Lower magnification SEM micrograph of the same device. (e) SEM micrograph of a beam that has been milled with a focused ion beam. The lack of large voids qualitatively confirms the density measurements. (f) Lower magnification micrograph of the same milled beam.

to maximize force or displacement. Potentially, higher force values are achievable; however, the force is as high as what is commonly achieved in electrostatic, electromagnetic, or piezoelectric actuators, which respectively have force outputs of: 0.001-1 mN, 0.0001-0.1 mN, and 0.01-1 mN [33].

Prior external field magnetic actuators have generated forces on the high end of electromagnetic actuators, but did not usually exceed 0.1 mN without unpractically large fields [33]. In these previous devices, the force was limited by the thickness of magnetic material that can be deposited on and adhere to compliant mechanisms made from non-magnetic materials. In contrast, our precise high-aspect-ratio compliant mechanisms were fabricated directly from magnetic materials resulting in an order of magnitude improvement in output force relative to these previous actuators. Additionally, it should also be noted that while this device has a footprint of 1.5 mm by 1 mm, the portion of the device responsible for the force is the proof mass which only has a small footprint of 0.5 mm by 1 mm.

V. Conclusion

Here, the CNT-M process was extended to fabrication of nickel structures by electroplating CNT forests. The composite material that results compares favorably to bulk nickel. It is significantly more compliant, but has comparable strength. Structures have been made from this material with aspect ratios greater than 20-1.

We have also fabricated an external field magnetic actuator that is significant because it achieves an order of magnitude improvement in force output over previous external field actuators, and demonstrates the ability to fabricate precise high-aspect-ratio compliant mechanisms out of nickel. This enables significantly higher performance external field magnetic actuators for applications including: biological implants, microrobotics for noninvasive surgery, and microfluidic mixers and pumps.

Acknowledgments

The authors would like to thank Andrew Davis and Ryan Badger, student researchers who did initial work with nickel plating.

References

[1] S. W. Pang, "High-aspect-ratio structures for MEMS," *MRS Bull.*, vol. 26, no. 4, pp. 307–308, Jan. 2011. [Online]. Available: http://journals.cambridge.org/abstractS0883769400023538

[2] E. H. Klaassen *et al.*, "Silicon fusion bonding and deep reactive ion etching: A new technology for microstructures," *Sens. Actuators A, Phys.*, vol. 52, nos. 1–3, pp. 132–139, Mar. 1996. [Online]. Available: http://www.sciencedirect.com/science/article/pii/0924424796801385

[3] C. K. Malek and V. Saile, "Applications of LIGA technology to precision manufacturing of high-aspect-ratio micro-components and -systems: A review," *Microelectron. J.*, vol. 35, no. 2, pp. 131–143, Feb. 2004. [Online]. Available: http://www.sciencedirect.com/science/article/pii/S0026269203002957

[4] W. Qu, C. Wenzel, A. Jahn, and D. Zeidler, "UV-LIGA: A promising and low-cost variant for microsystem technology," in *Proc. Conf. Optoelectron. Microelectron. Mater. Devices*, 1999, pp. 380–383. [Online]. Available: http://ieeexplore.ieee.org/lpdocs/epic03/wrapper.htm?arnumber=791668

[5] D. N. Hutchison *et al.*, "Carbon nanotubes as a framework for high-aspect-ratio MEMS fabrication," *J. Microelectromech. Syst.*, vol. 19, no. 1, pp. 75–82, Feb. 2010. [Online]. Available: http://ieeexplore.ieee.org/lpdocs/epic03/wrapper.htm?arnumber=5350708

[6] M. F. Aimi, M. P. Rao, N. C. MacDonald, A. S. Zuruzi, and D. P. Bothman, "High-aspect-ratio bulk micromachining of titanium," *Nature Mater.*, vol. 3, no. 2, pp. 103–105, 2004. [Online]. Available: http://www.nature.com/nmat/journal/v3/n2/abs/nmat1058.html

[7] C. Liu, *Foundations of MEMS*, 2nd ed., A. Gilfillan and A. Dworkin, Eds. Upper Saddle River, NJ, USA: Prentice-Hall, 2012.

[8] D. Niarchos, "Magnetic MEMS: Key issues and some applications," *Sens. Actuators A, Phys.*, vol. 106, nos. 1–3, pp. 255–262, 2003. [Online]. Available: http://dx.doi.org/10.1016/S0924-4247(03)00179-1

[9] L.-H. Lu, K. S. Ryu, and C. Liu, "A magnetic microstirrer and array for microfluidic mixing," *J. Microelectromech. Syst.*, vol. 11, no. 5, pp. 462–469, Oct. 2002. [Online]. Available: http://ieeexplore.ieee.org/lpdocs/epic03/wrapper.htm?arnumber=1038840

[10] M. Khoo and C. Liu, "Micro magnetic silicone elastomer membrane actuator," *Sens. Actuators A, Phys.*, vol. 89, no. 3, pp. 259–266, Apr. 2001. [Online]. Available: http://www.sciencedirect.com/science/article/pii/S0924424700005598

[11] J. W. Judy and R. S. Muller, "Magnetically actuated, addressable microstructures," *J. Microelectromech. Syst.*, vol. 6, no. 3, pp. 249–256, 1997.

[12] Y. W. Yi and C. Liu, "Magnetic actuation of hinged microstructures," *J. Microelectromech. Syst.*, vol. 8, no. 1, pp. 10–17, Mar. 1999. [Online]. Available: http://ieeexplore.ieee.org/lpdocs/epic03/wrapper.htm?arnumber=749397

[13] K. B. Yesin, K. Vollmers, and B. J. Nelson, "Modeling and control of untethered biomicrorobots in a fluidic environment using electromagnetic fields," *Int. J. Robot. Res.*, vol. 25, nos. 5–6, pp. 527–536, May 2006.

[14] J.-B. Mathieu, S. Martel, and G. Beaudoin, "Method of propulsion of a ferromagnetic core in the cardiovascular system through magnetic gradients generated by an MRI system," *IEEE Trans. Biomed. Eng.*, vol. 53, no. 2, pp. 292–299, Feb. 2006.

[15] X. Wei, C. H. Lee, Z. Jiang, and K. Jiang, "Thick photoresists for electroforming metallic microcomponents," *Proc. Inst. Mech. Eng., C, J. Mech. Eng. Sci.*, vol. 222, no. 1, pp. 37–42, Jan. 2008.

[16] C. Lee and K. Jiang, "Fabrication of thick electroforming micro mould using a KMPR negative tone photoresist," *J. Micromech. Microeng.*, vol. 18, no. 5, p. 055032, May 2008.

[17] H. Wang *et al.*, "A study on utilizing a chloride bath to electroform MEMS devices with high aspect ratio structures," *J. Micromech. Microeng.*, vol. 20, no. 11, p. 115024, Nov. 2010. [Online]. Available: http://stacks.iop.org/0960-1317/20/i=11/a=115024

[18] H. Yang and S.-W. Kang, "Improvement of thickness uniformity in nickel electroforming for the LIGA process," *Int. J. Mach. Tools Manuf.*, vol. 40, no. 7, pp. 1065–1072, May 2000. [Online]. Available: http://dx.doi.org/10.1016/S08906955(99)00107-8

[19] J. McGeough, M. Leu, K. Rajurkar, A. De Silva, and Q. Liu, "Electroforming process and application to micro/macro manufacturing," *CIRP Ann.-Manuf. Technol.*, vol. 50, no. 2, pp. 499–514, 2001.

[20] S. Basrour and L. Robert, "X-ray characterization of residual stresses in electroplated nickel used in LIGA technique," *Mater. Sci. Eng., A*, vol. 288, no. 2, pp. 270–274, Sep. 2000.

[21] Y.-H. Zhang, G.-F. Ding, Y.-L. Cai, H. Wang, and B. Cai, "Electroplating of low stress permalloy for MEMS," *Mater. Characterization*, vol. 57, no. 2, pp. 121–126, Aug. 2006.

[22] M. Staab, F. Greiner, H. F. Schlaak, and M. Schlosser, "Applications of novel high-aspect-ratio ultrathick UV photoresist for microelectroplating," *J. Microelectromech. Syst.*, vol. 20, no. 4, pp. 794–796, Aug. 2011.

[23] H.-K. Chang and Y.-K. Kim, "UV-LIGA process for high aspect ratio structure using stress barrier and C-shaped etch hole," *Sens. Actuators A, Phys.*, vol. 84, no. 3, pp. 342–350, Sep. 2000.

[24] K. Moulton *et al.*, "Effect of iron catalyst thickness on vertically aligned carbon nanotube forest straightness for CNT-MEMS," *J. Micromech. Microeng.*, vol. 22, no. 5, p. 055004, May 2012. [Online]. Available: http://iopscience.iop.org/09601317/22/5/055004/article/

[25] D. McKenna, "Tungsten infiltrated carbon nanotube forests as a framework for 3-d microfabrication," M.S. thesis, Dept. Phys. Astron., Brigham Young Univ., Provo, UT, USA, 2011. [Online]. Available: http://www.physics.byu.edu/thesis/archive/2011

[26] R. Hansen, "Mechanical and electrical properties of carbonnanotube-templated metallic microstructures," M.S. thesis, Dept. Phys. Astron., Brigham Young Univ., Provo, UT, USA, 2012. [Online]. Available: http://www.physics.byu.edu/docs/thesis/317

[27] H. Z. Wang *et al.*, "Reversible transformation of hydrophobicity and hydrophilicity of aligned carbon nanotube arrays and buckypapers by dry processes," *Carbon*, vol. 48, no. 3, pp. 868–875, Mar. 2010. [Online]. Available: http://www.sciencedirect.com/science/article/pii/S0008622309007143

[28] D. S. Jensen *et al.*, "Ozone priming of patterned carbon nanotube forests for subsequent atomic layer deposition-like deposition of SiO_2 for the preparation of microfabricated thin layer chromatography plates," *J. Vac. Sci. Technol. B, Microelectron. Nanometer Struct.*, vol. 31, no. 3, p. 031803, May 2013. [Online]. Available: http://scitation.aip.org/content/avs/journal/jvstb/31/3/10.1116/1.4801834

[29] B. H. Hanna *et al.*, "Mechanical property measurement of carbon infiltrated carbon nanotube structures for compliant micromechanisms," *J. Microelectromech. Syst.*, vol. 23, no. 6, pp. 1330–1339, Dec. 2014. [Online]. Available: http://ieeexplore.ieee.org/lpdocs/epic03/wrapper.htm?arnumber=6784315

[30] H. Majjad, S. Basrour, P. Delobelle, and M. Schmidt, "Dynamic determination of Young's modulus of electroplated nickel used in LIGA technique," *Sens. Actuators A, Phys.*, vol. 74, nos. 1–3, pp. 148–151, Apr. 1999. [Online]. Available: http://www.sciencedirect.com/science/article/pii/S0924424798003069

[31] S. M. Spearing, "Materials issues in microelectromechanical systems (MEMS)," *Acta Mater.*, vol. 48, no. 1, pp. 179–196, 2000. [Online]. Available: http://www.sciencedirect.com/science/article/pii/S1359645499002943

[32] A. M. Howatson, P. G. Lund, and J. D. Todd, *Engineering Tables and Data*. London, U.K: Chapman & Hall, 1972.

[33] D. Bell, T. Lu, and N. Fleck, "MEMS actuators and sensors: Observations on their performance and selection for purpose," *J. Micromech. Microeng.*, vol. 15, no. 7, p. S153, 2005. [Online]. Available: http://iopscience.iop.org/0960-1317/15/7/022

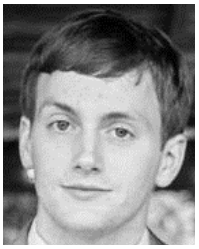

Lawrence K. Barrett received the B.S. degree in applied physics from Brigham Young University (BYU), Provo, UT, USA, in 2014. His research efforts focused on carbon nanotube templated microfabrication technology. During his undergraduate studies, he spent a summer with the Brookhaven National Laboratory, Upton, NY, USA, where he was involved in graphene growth. He is currently pursuing the M.S. degree in physics with a focus on ultrahigh capacity batteries with BYU.

Dallin J. Barton was born in Denver, CO, USA. He is currently pursuing the B.S. degree in physics from Brigham Young University (BYU), Provo, UT, USA. As an undergraduate student, he has been researching metal electroplating patterned carbon nanotube forests, including nickel electroplating for MEMS applications with BYU and copper electroplating for through-silicon via applications with the University of Alabama, Tuscaloosa, AL, USA.

Steven G. Noyce was born in Salt Lake City, UT, USA, in 1991. He is currently pursuing the B.S. degree in physics with Brigham Young University, Provo, UT, USA. He was recently a Physics Research Intern with Cornell University, Ithaca, NY, USA, where he was involved in developing a nanopore DNA sequencer with Dr. P. McEuen. His undergraduate research focuses on the development of porous resonator chemical sensors and self-assembled circuits using DNA origami metalization and carbon nanotube attachment.

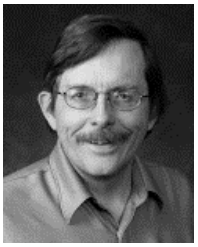

David D. Allred joined as a Faculty Member with Brigham Young University (BYU), Provo, UT, USA, in 1987, where he is currently a Professor of Physics and Astronomy. His research work includes thin-film/atomistic material deposition and characterization for applications, such as extreme ultraviolet optics and microfabrication at BYU. He has authored over 100 papers and holds 20 patents. He received the B.S. degree in chemistry from BYU, in 1971, and the Ph.D. degree in physics and physical chemistry from Princeton University, Princeton, NJ, USA, in 1977. He did post-doctoral research with Oak Ridge National Laboratory, Oak Ridge, TN, USA, and was a Research Associate with the Optical Sciences Center, University of Arizona, Phoenix, AZ, USA. He was with Energy Conversion Devices Inc., Troy, MI, USA, for seven years.

Richard R. Vanfleet joined the Department of Physics and Astronomy, Brigham Young University (BYU), Provo, UT, USA, in 2003. He currently serves as the Chair of the Department of Physics and Astronomy. His research interests include the atomic and nanoscale characterization of materials, phase transitions in nanoparticles, carbon nanotube templated microfabrication, and other applied problems.

He received the B.S. degree from BYU, and the M.S. and Ph.D. degrees from the University of Illinois at Urbana—Champaign, Champaign, IL, USA, all in physics. He was a Post-Doctoral Researcher with the School of Applied and Engineering Physics, Cornell University, Ithaca, NY, USA, from 1997 to 1999. He has been a Faculty Member with the University of Central Florida, Orlando, FL, USA, and was a Visiting Professor with the University of Cape Town, Cape Town, South Africa, and the University of Western Cape, Cape Town.

Robert C. Davis joined as a Faculty Member with Brigham Young University (BYU), Provo, UT, USA, in 1998, where he is currently a Professor of Physics. His research includes the development of the fabrication technique carbon nanotube templated microfabrication (CNT-M) at BYU. The CNT-M is being applied to a wide variety of applications from chemical separations to microactuation with Researchers at BYU. His research in microfabrication and nanofabrication has resulted in 85 publications and 14 patents.

He received the B.S. degree in physics from BYU, in 1989, and the Ph.D. degree in physics from the University of Utah, Salt Lake City, UT. He was a Post-Doctoral Researcher with Cornell University, Ithaca, NY, USA, from 1996 to 1998.